HHS Public Access

Author manuscript

J Biomed Mater Res A. Author manuscript; available in PMC 2023 July 06.

Published in final edited form as:

J Biomed Mater Res A. 2022 July ; 110(7): 1356–1371. doi:10.1002/jbm.a.37378.

Pegylated insulin-like growth factor-1 biotherapeutic delivery promotes rotator cuff regeneration in a rat model

Anupama Prabhath[1,2,3], **Varadraj N. Vernekar**[1,2], **Caldon J. Esdaille**[1], **Ellen Eisenberg**[4], **Amir Lebaschi**[2], **Mary Badon**[1], **Amir Seyedsalehi**[1,2,3], **Godwin Dzidotor**[1,2,5], **Xiaoyan Tang**[1,2,6], **Nathaniel Dyment**[7], **Stavros Thomopoulos**[8,9], **Sangamesh G. Kumbar**[2,3,6], **Alix Deymier**[3], **Eckhard Weber**[10], **Cato T. Laurencin**[1,2,3,5,6]

[1]Connecticut Convergence Institute for Translation in Regenerative Engineering, Farmington, Connecticut, USA

[2]Department of Orthopaedic Surgery, UConn Health, Farmington, Connecticut, USA

[3]Department of Biomedical Engineering, UConn Health, Farmington, Connecticut, USA

[4]Department of Pathology and Laboratory Medicine, UConn Health, Farmington, Connecticut, USA

[5]Department of Chemical Engineering, University of Connecticut, Storrs, Connecticut, USA

[6]Department of Material Science and Engineering, University of Connecticut, Storrs, Connecticut, USA

[7]McKay Orthopaedic Research Laboratory, Perelman School of Medicine, University of Pennsylvania, Philadelphia, Pennsylvania, USA

[8]Department of Orthopedic Surgery, Columbia University, New York, New York, USA

[9]Department of Biomedical Engineering, Columbia University, New York, New York, USA

[10]Novartis Institutes for BioMedical Research (NIBR), Basel, Switzerland

Abstract

Tears in the rotator cuff are challenging to repair because of the complex, hypocellular, hypovascular, and movement-active nature of the tendon and its enthesis. Insulin-like Growth Factor-1 (IGF-1) is a promising therapeutic for this repair. However, its unstable nature, short half-life, and ability to disrupt homeostasis has limited its clinical translation. Pegylation has been shown to improve the stability and sustain IGF-1 levels in the systemic circulation without disrupting homeostasis. To provide localized delivery of IGF-1 in the repaired tendons, we encapsulated pegylated IGF-1 mimic and its controls (unpegylated IGF-1 mimic and recombinant

Correspondence: Cato T. Laurencin, Department of Material Science and Engineering, University of Connecticut, Storrs, CT, USA. laurencin@uchc.edu.

CONFLICT OF INTEREST

Eckhard Weber, Ph.D. is an employee of Novartis Institute for Bio-Medical Research (NIBR), Basel, Switzerland. Cato T. Laurencin, M.D., Ph.D. received grant funding from NIBR (G600795) for conducting this work. Cato T. Laurencin, M.D., Ph.D. serves on the boards of MiMedx, Alkermes, BioBind, and Healing Orthopaedic Technologies-Bone.

SUPPORTING INFORMATION

Additional supporting information may be found in the online version of the article at the publisher's website.

human IGF-1) in polycaprolactone-based matrices and evaluated them in a pre-clinical rodent model of rotator cuff repair. Pegylated-IGF-1 mimic delivery reestablished the characteristic tendon-to-bone enthesis structure and improved tendon tensile properties within 8 weeks of repair compared to controls, signifying the importance of pegylation in this complex tissue regeneration. These results demonstrate a simple and scalable biologic delivery technology alternative to tissue-derived grafts for soft tissue repair.

Keywords

delivery; enthesis; IGF-1; insulin-like growth factor-1; pegylation; polycaprolactone; polylactic acid; polylactide; rotator cuff; tendon

1 | INTRODUCTION

Rotator cuff injuries are a significant health care burden in the United States with over 200,000 repair procedures done annually at an estimated $474 million dollars spent on related healthcare costs.[1,2] Despite improvements in surgical repair techniques, the failure rate of these repairs varies widely from 20% to 95%.[3,4] Failure occurs at the suture-repair tissue interface because the tendon and its fibrocartilaginous interface to bone (enthesis) heals poorly with weak fibrous tissue.[5,6] To improve surgical repair outcomes tissue-derived grafts are employed. However, limited availability, risk of infection, unpredictable graft degradation, and non-specific graft induction ability limit the widespread use of these grafts.[7] Likewise, the use of stem cells in rotator cuff repair models shows promise however their large-scale manufacturing and delivery for clinical application is challenging.[7–10,12,13] Growth factors on the other hand are easier to deliver, yet their short half-life requires multiple injections reducing patient compliance and is unstable in aqueous environments. Therefore, there is a need to protect the growth factors and provide sustained release to improve its delivery in the clinic. Delivery matrices made from synthetic polymers can be tailored for sustained release of growth factors and manufactured at scale for clinical translation.

Several growth factors are expressed in healing rotator cuff tissue and Insulin-like Growth Factor-1 (IGF-1) is highly expressed through-out the repair process.[15–17] IGF-1 plays a key role in inflammation resolution and extracellular matrix (ECM) synthesis.[18,19] However, previous studies have shown that although tendon lesions were filled with new collagenous tissue upon IGF-1 injection, the tendon biomechanical failure loads did not improve.[19] This indicates the need for sustained presence of IGF-1 for augmenting new collagen tissue formation and maturation to provide superior tissue function in the repaired rotator cuff. However, since IGF-1 has a short half-life (~10 min in plasma) multiple injections would be required to achieve sustained therapeutic dose.[20] Moreover, IGF-1 being a close homologue of insulin can bind to insulin receptors increasing risk of hypoglycemia and growth hormone suppression.[21] Pegylation of IGF-1 has been shown to maintain sustained anabolic activity[21] without causing adverse effects of hypoglycemia and growth hormone suppression by limiting fast association of IGF-1 ligand to IGF-1- and Insulin- receptor, and IGF-I-binding proteins.[21–23] We therefore utilized a pegylated IGF-1 mimic (PEG-IGF-1m), which is

a synthetic peptide that has been engineered to provide site(s) for pegylation. To ensure controlled, localized, and protected delivery of PEG-IGF-1m, the growth factor needs to be encapsulated in a carrier matrix. Common biodegradable poly(lactic-co-glycolic acid)-based delivery systems is limited by burst release, brittle nature, and acidic degradation byproduct accumulation which can cause loss of encapsulated biologic stability.[24] We therefore developed an elastomeric co-polymeric matrix from poly(L-lactide)-co-poly(ε-caprolactone) (PLA-CL), which showed controlled, conformationally stable macromolecular release and degradation with less acidic byproduct accumulation. This matrix also maintained pliability for implantation in the movement-active rotator cuff.[25] In the current study, a PLA-CL formulation of 45 kDa (M_n) with a lactide-to-caprolactone ratio of 27:73 we optimized previously[25] was implemented to encapsulate and deliver pegylated- and unpegylated-Insulin-like Growth Factor-1 Mimics (PEG-IGF-1m and IGF-1m) and recombinant human Insulin-like Growth Factor-1 (rh-IGF-1) control in a pre-clinical animal model of rotator cuff repair. This molecular weight and higher CL ratio were chosen to allow faster water penetration (from increased rubbery domains of CL) and thereby faster hydrolytic degradation without acidic degradation product accumulation; a higher CL ratio would also help minimize burst release and generate pliable elastic matrices that supports surgical implantation in the rotator cuff.[25]

Histology and microCT of the isolated tissues were used to assess tissue microstructure and uniaxial tensile test was used to assess tissue biomechanical function. We found that pegylated-IGF-1 mimic (PEG-IGF-1m) biotherapeutic delivery showed structural regeneration of the tendon-enthesis with improved collagen organization and maturity, columnar arrangement of fibrochondrocytes with significant recovery of the tendon failure mechanics and tensile properties within 8 weeks of repair. Our work reports the first demonstration of the use of a sustained and controlled IGF-1 biotherapeutic delivery technology in the rotator cuff resulting in both structural regeneration of enthesis and biomechanical recovery of native tendon material properties. The pegylated IGF-1m matrix sustained release system has the potential for prolonged localized delivery of IGF-1 in the clinic over-coming dosing limitations and the adverse effect on insulin and growth hormone homeostasis.

2 | MATERIALS AND METHODS

To model growth factor release, we encapsulated a model protein, bovine serum albumin (BSA, 5 wt.%, Sigma-Aldrich, St. Louis, MO) in several formulations of the PLA-CL copolymer with molecular weights (M_n) ranging from 15 to 45 kDa and lactide-to-caprolactone ratios ranging from 15:85 to 30:70 (LA:CL). The PLA-CL copolymers were custom fabricated to achieve as close to our design specification as possible by PolySciTech, Akina, Inc., West Lafayette, IN. Casting solution concentration in the range of 5–20 polymer wt.% in dichloromethane (DCM, Fisher Scientific, Hampton, NH) was used to fabricate 300 μm thick protein-loaded matrices via film casting (4°C, 48 h). The formulation of 45 kDa (M_n) and 27:73 LA:CL ratio at 20 wt.% casting solution concentration in DCM that resulted in the best quality matrices and macromolecular release profiles was selected for encapsulation of the IGF-1 biotherapeutics in the in vivo rotator cuff repair studies. In the matrix degradation and macromolecular (BSA) release studies control matrices did

not contain the encapsulated protein (w/o BSA). All chemicals and materials used in this study were obtained from Fisher Scientific, Hampton, NH, unless specifically mentioned otherwise; they were of high purity research grade and used as received.

2.1 | Protein-encapsulated matrix fabrication

Protein-encapsulated PLA-CL matrices were fabricated using a solvent-casting process using previously optimized methods.[25] For assessing protein encapsulation and release, pulverized lyophilized protein, Bovine Serum Albumin (BSA) was dispersed at 5 wt.% protein vs. polymer in pre-dissolved PLA-CL solutions in dichloromethane (DCM) and vortexed and sonicated at 4°C for approximately 5 min each until uniform dispersions were obtained. Protein-dispersed polymer solutions in dichloromethane (DCM) at 5, 10, and 20 wt./vol.% polymer concentrations were poured on to 60 mm diameter Teflon evaporation dishes (Fisher Scientific, Hampton, NH) and placed under vapor saturated conditions on a leveled platform at 4°C for 2 days. Vapor saturated conditions, created by covering each Teflon dish with a lid, slowed the evaporation process aiding in the formation of structurally intact films without defects from the 45 kDa (M_n) 27:73 LA:CL ratio polymer at 20 wt.% casting solution concentration (Figure 1A). THE REsulting copolymer film was dried for a minimum of 2 days at room temperature under vacuum to ensure removal of any residual solvent, stored temporarily in a desiccator, and quickly used for experimentation. Complete drying of film matrices was ensured by lack of significant measured weight-change over this period and up to 1 week when dried under vacuum at room temperature, and comparing to film matrix weight-change after lyophilization, which were all indistinguishable from each other. For the in vivo studies, pulverized lyophilized rh-IGF-1 and pegylated IGF-1 biotherapeutic were both independently loaded at 5 wt%, and IGF-1m was loaded at 2.4 wt% by dispersed in 45 kDa (Mn) poly (L-lactic acid)-co-poly(ε-caprolactone) (PLA-CL, 27:73) and dissolved in dichloromethane (DCM) to form thin film matrices using the same protocol as mentioned above. Both the protein and the growth factor-loaded films were cut to obtain 3 mm × 3 mm matrices. The mean thickness of each film was 300 μm, which provided adequate volume to load the protein on the small footprint of 3 mm × 3 mm that could be sutured with reasonable ease on the tendon during rotator cuff repair in the in vivo studies. It also allowed unhindered existence of the matrix within the narrow bursal clearance space between the rotator cuff tendon and the acromion upon implantation without significant impingement, an acceptable degradation rate, and controlled protein release.

2.2 | Protein release and secondary structure analysis

Model protein BSA release was monitored by incubating the matrices in 7.4 pH 1X phosphate buffered saline (PBS, spiked with 0.05 wt.% sodium azide and 0.01% Brij 35) at 37°C under gentle agitation over the course of 4 and 8 weeks, respectively. BSA was chosen as a model factor for delivery from biodegradable polymeric system as it has precedence in use as a model factor in traditional PLGA-based controlled release systems and allows comparison of release kinetics and degradation conditions with previously reported literature.[24,26] Additionally, the primary test growth factor candidate in this study, the PEG-IGF-1m has a molecular weight 41.2 kDa, (~11.2 kDa IGF-1-Mimic +30 kDa PEG) relatively closer to that of BSA. PBS mimicked the physiological pH and osmolality conditions. Evaporative losses were minimized during the study by sealing the incubation

vials tightly with parafilm and conducting the study in a humidity saturated environment. The model protein released from the matrices was measured in triplicate at 0, 0.5, 1, 3, and 8 h as well as at 5, 10, 14, 24, and 28 days. Briefly, at each time-point, the release buffer was removed from the matrix incubation vial and used for protein measurements (quantitation and conformation). The minimal necessary release buffer volume was included in each vial to allow release protein concentration at detectable levels, yet large enough to maintain sink conditions. Our experimental procedure measured absolute release.

The concentration of protein released within the sample incubation buffer was assessed at the designated time points using the bicinchoninic acid (BSA) assay (Fisher Scientific, Hampton, NH). Standard curves were constructed using protein standards assayed concurrently with the released protein. Using this calibration, the unknown protein concentration was determined spectrophotometrically. Likewise, the conformation of released proteins was measured using Circular Dichroism (CD) spectroscopy in the far-UV under controlled temperature conditions (Jasco Spectroscopic Co., Japan). The CD data are presented as ellipticity, calculated based on the protein concentration and the path length of the cell.

2.3 | Matrix microstructure

The matrix microstructure was visualized in 3-D using the fluorescent dye, fluorescein (Sigma-Aldrich, St. Louis, MO) and confocal laser scanning microscopy (Zeiss, Germany). To do this, the matrices were first saturated with an ethanolic solution containing 1 mg/ml fluorescein at room temperature. The matrices were then dried in a vacuum at room temperature for 3 days and rehydrated in PBS buffer supplemented with 0.1 mg/ml of fluorescein at the time of imaging. A 100% ethanolic solution was used for saturating the matrices with fluorescein because of the solubility of fluorescein in this solvent and insolubility of the protein BSA in it. Green fluorescence from accessed fluorescein lit up all fluid accessible regions in the polymeric matrix microstructure including the protein regions that were accessible. To determine pore size, the image analysis of z-sections of the matrix was conducted using imageJ software. The images were converted to binary images and the pixel intensity was thresholded to delineate pores, whose brightness is lower than those occupied by the polymeric phase. The pore sizes were determined and plotted as frequency distribution in Figure S1.

2.4 | In vivo rotator cuff repair study design

The protocol for all the in vivo studies was approved by the Institutional Animal Care and Use Committee (IACUC) of the University of Connecticut Health Center. National Institute of Health (NIH) guidelines for the care and use of laboratory animals (NIH Publication #85–23 Rev. 1985) were observed. To assess histological repair outcomes, 28 age-matched male Sprague Dawley rats (475 ± 25 g, Charles River, Wilmington, MA) underwent unilateral supraspinatus tendon detachment and trans-osseous repair at the insertion site. The animals were randomly divided into four groups (n = 3/group at 4 weeks and n = 4/group at 8 weeks) for repair via: (i) suture only (repair control), (ii) suture with bare matrix (matrix control), (iii) suture with IGF-1-mimic-loaded matrix (IGF-1m matrix), and (iv) suture with pegylated-IGF-1-mimic-loaded matrix (PEG-IGF-1m matrix) (Figure S2). Animals were

allowed 4 or 8 weeks of cage activity post repair. In addition, uninjured animals ($n = 7$) and sham (surgical approach alone) animals ($n = 7$) served as native tissue controls. An a priori power analysis using semi-quantitative histology data from a comparable rat rotator cuff study[9] was performed. This resulted in a sample size of 3–4 per treatment with a power of 80% for a p-value of .05 determining significance. Biomechanical repair outcomes were assessed using the same model. The animals were randomly divided into native tissue control, repair control, recombinant IGF-1 (rh-IGF-1), and PEG-IGF-1m groups ($n = 6–8$/group/time point at 4 and 8 weeks) (Figure S2).

2.5 | Rotator cuff tear repair surgery and matrix implantation procedure

Rats were placed in a ventral/lateral recumbency position after sterile preparation of the surgical site and induction of anesthesia. The left shoulder was adducted, and a 1–3 cm subcutaneous incision centered perpendicular to the acromial arch was made, followed by minimal dissection of the deltoid muscle along the lateral border of the acromion exposed the acromioclavicular (AC) joint. The AC joint was gently elevated using a skin hook to expose the underlying supraspinatus tendon (SST) insertion (Figure 2A). A double-needled 5–0 Prolene suture (Covidien, Dublin, Ireland) was used to create a modified Mason Allen suture starting at the mid-substance of the SST and completing the configuration with the other needle and tagging the tendon (Figure 2A). The SST was completely detached from the humerus at the insertion using a #11 blade to create a full-thickness defect. (Figure 2B). The tendon footprint was prepared using a 0.5 mm diameter surgical burr (Fine Science Tools, Foster City, CA) to remove any residual fibrocartilage. A posterio-anterior trans-osseous bone tunnel was next created in the humeral head approximately 2 mm lateral to the articular surface and 2 mm distal to the supraspinatus footprint using a 0.5 mm Kyocera drill bit (Grainger, Lake forest, IL) (Figure 2C). The tendon-tagging sutures were then passed through the bone tunnel and tied to the humerus, re-approximating the torn tendon back onto its prepared footprint (Figure 2C). This trans-osseous technique compresses the tendon to the footprint with a broad area of fixation, minimizes avulsion failures, and improves fixation strength and footprint bone preservation.[27] For matrix and growth factor-augmented repairs, the tied suture ends from the footprint-re-approximated tendon were sub-chondrally anchored on the anterior and posterior sides of the SST insertion (Figure 2D) and then used to create a cross mattress stitch on the engineered matrix (Figure 2E), which was thereby independently secured on the bursal side of the SST insertion in a “piggy-back” manner (Figure 2F). The deltoid was reflected over the humerus and closed and the overlying skin was approximated and closed with an absorbable Vicryl suture (Ethicon, Somerville, NJ). For sham surgery controls only the surgical approach and wound closure procedure was followed.

2.6 | Rotator cuff tissue preparation for histology and biomechanics

The animals were euthanized at 4 and 8 weeks using carbon dioxide inhalation. For histology, the harvested rotator cuff tissue comprising of the humeral head with the attached supraspinatus and infraspinatus tendon-muscle units supported on the scapula was adducted and tied at approximately 60° to maintain the orientation of the rotator cuff tendon constant across groups (Figure S3A). Samples were fixed in 10% Neutral Buffered Formalin, decalcified in DeltaCAL slow decalcifier (Mercedes Scientific, Lakewood Ranch,

FL), and embedded in paraffin using standard techniques modified for the tissue (Figure S3B). Samples to be embedded in PMMA were stored in 70% ethanol at 4°C until the time of embedding (Figure S3B). Coronal sections 5 μm thick at the same depth optimized by observing anatomical landmarks of glenoid and the shape of the growth plate and the humeral head were selected for all histological staining and analyses. Sections were stained with hematoxylin and eosin (HE), Masson's trichrome (MT), Safranin O (SO), and Picrosirius Red (PR) for assessing tissue morphology and quality, fibrocartilage formation, and collagen fiber organization, respectively. Imaging of colorimetric stained sections was done under an in-house light microscope (Leica Dmi8, Wetzlar, Germany). An inverted light microscope (Olympus IX73SC, Tokyo, Japan) fitted with a circular polarizer was used for imaging Picrosirius red-stained sections. For the assessment of mineralization, PMMA-embedded sections were used and stained with Von Kossa (VK) to visualize the mineral and toluidine blue (TB) to visualize cells and matrix, respectively.

For biomechanical assessments, only the supraspinatus muscle tendon-unit was removed from the scapula keeping the attachment site to the humerus intact.

2.7 | Histomorphometric assessment of tendon-to-bone insertion maturity

Histomorphometry scores for inflammation (granulation tissue, vascularity, and cellularity) and insertion integrity (continuity, regularity, and fibrocartilage) were graded blindly by a trained institute pathologist using a modified methodology adapted from a tendon-to-bone interface maturity scoring scale described previously (Table 1).[12,28] Overall, Masson's Trichrome-stained images were obtained under a 40X objective at the tendon-to-bone interphase for the qualitative assessment of granulation tissue, vascularity, and cellularity at 4 and 8 weeks after repair. Percentage granulation tissue was assessed specifically by identifying the densely cellular and vascular area stained dark red in MT-stained sections under 10× objective.[29] This area was estimated with respect to the total callus area of the tissue sample to obtain percentage of granulation tissue within each sample. The SO-stained sections were visualized at 10X objective and then at 10× objective × 0.25 numerical aperture to assess continuity, regularity, and fibrocartilage, respectively (Table 1). Continuity is defined by a seamless transition of cells from the soft tissue to bone with the absence of a distinct boundary between soft tissue and bone (Figure S4A–a). Regularity is defined by the presence of cells that have a common pattern or orientation in the way they are arranged at the insertion (Figure S4B–a). Fibrocartilage is defined by the presence of lacunae-presenting rounded cells with pink/red pigmentation surrounding the cells (metachromasia) signifying the presence of the characteristic glycosaminoglycan matrix (Figure S4C). ImageJ based histomorphometry tools were used to measure percentage metachromasia, collagen birefringence, collagen fiber diameter and cellular orientation at the tendon-to-bone interface. For percentage metachromasia, Safranin O-stained sections were imaged at 40× objective, and the total area of new fibrocartilage formation was calculated by measuring the metachromatic regions in each specimen using a color thresholding function in the ImageJ software (National Institutes of Health, Bethesda, Maryland) using previously established methods.[8] This metachromatic area was divided by the total area of the enthesis to get the ratio of metachromasia in each sample. To measure collagen birefringence, Picrosirius Red-stained sections imaged under a polarizing microscope (Leica Dmi8, Wetzlar, Germany) at

40× objective were used. Two-to-three ROIs of 250 μm^2 dimension were demarcated at the tendon and its enthesis and converted to 8-bit gray scale image (black, 0; white, 255); the gray scale values were measured and recorded.[8] Picrosirius Red-stained sections were also used to estimate collagen fiber diameter from its hue which changes with decreasing fiber diameter as Red (thick) > Orange > Yellow > Green (thin). To determine the proportion of different colored collagen fibers, the polarized images of PSR stained sections was resolved into its hue, saturation and value components using an ImageJ.[30] Only the hue component was retained and a histogram of hue frequency was obtained from the resolved 8-bit hue images which contain 256 colors. The following hue definitions were used; red 2–9 and 230–256, orange 10–38, yellow 39–51, green 52–128. The number of pixels within each hue range was determined and expressed as percentage of the total number of collagen pixels. Visualization and measurement of cellular orientation was done using the OrientationJ plug-in in ImageJ using previously established methods of images of Safranin O-stained sections (Figure S6A,B, respectively).[31] Cell orientation is demonstrated using an orientation map function which shows a hue-saturation-brightness (HSB) color-coded map to show the angles of the oriented cells (Figure S6A). Coherency Coefficient (CC) gives the degree to which the cells are aligned with-respect-to each other (Figure S6B), and this value lies in the range of 0–1, with 0 being completely isotropic with no dominant cellular direction and 1 being completely anisotropic with all cells oriented in a particular direction.

2.8 | Bone morphometry

From the biomechanics samples, supraspinatus tendon-muscle units with humerus intact were isolated, wet in a PBS-soaked gauze and stored at 4°C for scanning using microcomputed tomography (μCT40, Scanco Medical AG, Bassersdorf, Switzerland) within 24 h. The humerus was potted in a cryovial containing 10% agarose gel ensuring the supraspinatus tendon-muscle hung from it without touching the walls of the cryovial. The scans were done at medium resolution at an energy of 55 kV, intensity of 145 μA, 1000 projections, and 300 ms integration. The images were segmented to measure tendon minimum cross-sectional area and trabecular bone morphometry parameters. The trabecular bone was segmented proximal to the growth plate in all samples. A trabecular morphometry segmentation program was used to determine bone mineral density (BMD), bone volume fraction (BV/TV), trabecular number (Tb. N), trabecular thickness (Tb. Th), and trabecular spacing (Tb. Sp).

2.9 | Biomechanics

The supraspinatus muscle was carefully removed from the tendon using the blunt side of a #15 blade after microCT scanning. The humerus was affixed into a custom 3-D printed bone fixture designed by the Thomopoulos lab. Likewise, the tendon was secured in an optimized custom 3-D printed fixture, which minimizes grip failure of rat tendons without using any adhesives. The unit was then affixed to a 250 N load cell on a mechanical testing set up (Mach-1 V500C, MA001, Biomomentum, Canada) and the samples were submerged in a saline bath at room temperature to undergo quasistatic uniaxial tensile testing. The sutures were cut prior to testing. The samples were preloaded to 0.1 N, followed by ramp-to-failure at 0.1% strain/s. A camera attached to the testing setup was used to determine the strain from the displacements relative to the initial gauge length and to visually determine

the mode of failure. The minimal cross-sectional area measured from the microCT was used to calculate stress. Structural properties, failure load, stiffness, and work to failure (area under the curve through failure load), were determined from the load-deformation curves.[32] Material properties, strength, modulus, resilience (area under the curve through yield), and toughness (area under the curve through failure), were determined from stress–strain curves.[32] After the biomechanical assessments, the samples were scanned again using microCT to determine the mode-of-failure.

2.10 | Statistical analysis

All statistical analyses were performed on Prism 9 (GraphPad Software, San Diego, CA). Two-way analyses of variance (ANOVA) were performed to evaluate effects of treatment (repair controls, rh-IGF-1, PEG-IGF-1m) and time (4 and 8 weeks). Tukey's post hoc test was used when the 2-way ANOVA test resulted in significance ($p \leq .05$) between the treatment groups. Šídák's multiple comparisons post hoc test was used when the 2-way ANOVA test resulted in significance ($p \leq .05$) between the time-points. Three levels of significance were used to demonstrate the magnitude differences: $p \leq .05$, $p \leq .01$, and $p \leq .001$, respectively.

3 | RESULTS

3.1 | Engineered matrices were porous and allowed controlled release of structurally intact model protein

Toward ultimately testing the implantable delivery matrices for the therapeutic release of IGF-1 mimics in vivo, the matrices prepared via a thin-film fabrication process were initially tested for the encapsulation and release of the model protein Bovine Serum Albumin (BSA) in vitro. These formed films were highly pliable and approximately 300 μm thick (300 ± 30 μm) (Figure 1A). Confocal Microscopy revealed that these films had a highly porous microstructure (~90% pore surface area <50 μm^2) that appeared to form because of aggregation of discrete microspherular units (diameters between 20 and 100 μm) (Figure 1B) (Figure S1), and which occupied the entire thickness of the film. This is due to the crystallization from solution that occurs when the solvent evaporation rate is low enough for polymer macromolecules to diffuse to the crystal growth front and overcome the energy barrier of deposition forming spherulites as described previously.[25,33] Matrices prepared from a 20 wt.% solution of 45 kDa PLA-CL (27:73) were structurally intact, degraded with ~30% reduction in molecular weight in the first 4 weeks with minimal pH change in vitro and underwent remodeling without eliciting excessive inflammatory reaction in vivo.[25] Based on these results, 20 wt.% solution of 45 kDa PLA-CL (27:73) matrices were chosen for further experimentation. Based on spectrophotometric measurements of the released protein, these matrices released the BSA payload in an initial low burst of less than 15% of loading within the first 24 h, followed by controlled and continuous release over 4 weeks (Figure 1C). The secondary structure of the protein was preserved during the protein encapsulation and release processes even after 8 weeks of incubation at 37°C in the release buffer, with the released BSA showing closely matching double-minima of the predominantly α-helical secondary structure of BSA around 210 and 220 nm in circular dichroism measurements (Figure 1D).[34] These data are consistent with our

pH measurements of the release buffer, which remained unaltered from physiological pH throughout the duration of the study. Since the secondary structure of the encapsulated BSA was preserved through 8 weeks in physiological conditions, it was assumed that the optimized polymeric matrix formulation would also preserve the secondary structure of the encapsulated IGF-1 biotherapeutics and was selected for further experiments. Since the matrix in this study was designed only to serve a drug delivery and not intended to have a load-bearing function, no mechanical testing was performed.

3.2 | Reduced fibrosis and improved structural regeneration of the tendon and transitional fibrocartilaginous enthesis via pegylated-IGF-1 mimic delivery

A lyophilized rh-IGF-1, IGF-1 mimic (IGF-1m), and its pegylated-version (PEG-IGF-1m) were encapsulated independently in the optimized PLA-CL matrix, which was implanted on the bursal side of the supraspinatus tendon-enthesis following complete transection of the tendon at the enthesis, debridement of the tendon foot-print at the enthesis, and trans-osseous repair for reattachment of the transected tendon (Figure 2). The implanted matrices remained localized at the repair site even after 8 weeks as evaluated previously.[25] Masson's trichrome staining was used to assess the tissue repair response. Specifically, the rotator cuff tissue was assessed for overall tissue hypertrophy, granulation tissue, vascularity, cellularity, and new collagen deposition in all groups. At 4 weeks, new hyper-cellular and vascular granulation tissue was seen interspersed with neotendinous tissue indicative of the reparative process underway in the tendon-to-bone interface region in all the matrix-augmented groups (Figure 3A–C). The tendon-to-bone interface did not show any gap formation in any of the repaired groups (Figure 3A–C). By 8 weeks, the granulation tissue at the tendon-to-bone interface had remodeled into more organized tissue in all matrix augmented groups indicating that tissue healing response at this site was also minimally affected, if at all, by the byproducts of matrix degradation by this time point (Figure 3D–F). The collagen fibers and the cells within the organized interfacial tissue were distinctly denser and more aligned, with the rounder cell morphology throughout the tendon-to-bone boundary in the PEG-IGF-1m treatment group (Figure 3F) compared to the matrix control (Figure 3D) and IGF-1m (Figure 3E) groups. Overall, cellularity was increased in all the surgical repair groups at 4 weeks (when compared to sham controls) (Table 2), and gradually reduced to moderate levels by 8 weeks, with the PEG-IGF-1m treatment group (Figure 4D,D_i, Table 2) showing reduced cellularity at the insertion than all the other repair groups (Figure 4B,B_i,C,C_i) (Table 2). On the other hand, granulation tissue and vascularity were higher in the matrix control group when compared to the other groups at 4 weeks and reduced to repair control levels by 8 weeks (Table 2).

The presence of fibrocartilage at the interface at 8 weeks was further assessed using Safranin O staining. Whereas, granulation tissue with infiltrating fibroblasts was seen at the repair interphase in all groups at 4 weeks in the Masson's trichrome-stained sections (Figure 3, Figure S7), repair groups showed improved remodeling into more organized interfacial tissue by 8 weeks in the Safranin O-stained sections (Figure 4). However, the PEG-IGF-1m group showed the most reorganization of the repaired tissue interface into fibrocartilage, with the reestablishment of the characteristic columnar arrangement of fibrochondrocytes,

emergence of metachromasia surrounding these chondro-typic cells, and the tidemark (Figure 4D,D_i), which were comparable to the native enthesis (Figure 4A,A_i).

Collagen organization was qualitatively and semi-quantitatively assessed from images of Picrosirius Red-stained sections that appear with characteristically different coloration caused by the birefringence of polarized light depending on the degree of molecular order in collagen. Improvement in tendon collagen organization was seen particularly in the PEG-IGF-1m treatment group compared to the repair control, matrix control, and IGF-1m treatment groups by 8 weeks as noted by its significantly higher collagen birefringence by this time point (Figure 5D). The PEG-IGF-1m group also showed inter-digitating aligned collagen fibers anchoring into the cortical bone at both 4 and 8 weeks, as indicated by white arrows in the Picrosirius Red-stained polarized light images in Figure 5B–d and h. The collagen fiber diameter of the treated groups was assessed based on the differential birefringence color (red, orange, yellow, or green) resulting from the differential binding of picrosirius dye to collagen fibers. The larger, more mature collagen fibers appear bright red when bound to the picrosirius dye and with decreasing fiber diameter they exhibit orange, yellow, and green (newly deposited collagen) birefringence. The native tendon showed 34X and 1.73X increase in the larger diameter red and orange collagen fibers, respectively, as the rats matured from 4 to 8 weeks (Figure S5). Distinct maturation was seen in the PEG-IGF-1m-treated groups which showed 88% smaller diameter green collagen fibers at 4 weeks which matured to 77% and 3% larger diameter orange and red fibers, respectively, by 8 weeks (Figure S5). Cellular orientation was calculated from ImageJ-processed images (OrientationJ plugin) of Safranin O-stained sections (Figure 5C) in terms of a coherency coefficient (or in other words the degree of anisotropy of cells with respect to each other). A coherency coefficient of 1 indicates perfect anisotropy of cells and 0 indicating isotropy. Cellular orientation (anisotropy) was improved significantly in the IGF-1m and PEG-IGF-1m treatment groups compared to the matrix control at 8 weeks (Figure 5C,E). Overall, the PEG-IGF-1m treatment group showed distinct improvements in the healing response with improved structural regeneration of the tendon in terms of tissue-typic aligned collagen fiber anchoring into bone and improved cellular orientation at the enthesis as seen in the images in Figures 3–5. This response was also reflected in the semi-quantitative histomorphometric scoring, which showed an improved insertion maturity score in the PEG-IGF-1m treatment group, closest to that of the native enthesis, compared to all the other matrix-augmented groups by 8 weeks (Table 2).

3.3 | Regenerative versus scar tissue healing in PEG-IGF-1m versus rh-IGF-1 treatment groups resulting in differential failure mode and mechanics in the enthesis

To further evaluate the biomechanical properties of the PEG-IGF-1m treatment repaired tissue, which showed improved structural healing, we conducted a second animal study designed to compare this group to the standard recombinant human IGF-1 (rh-IGF-1) delivered via the same engineered matrix and surgical repair controls. Distinctly different repair responses were noted in the rh-IGF-1 and PEG-IGF-1m treatment groups, respectively. The former healed with a scar-like tissue characterized by a larger cross-sectional area (CSA) that was approximately 200% higher in comparison to native tendon (Figure 6A–b,e, B), whereas the latter had a more tendon-typic shiny-whitish appearance

with a smaller CSA compared to the rh-IGF-1 treatment group, but was still approximately 80% larger than native tendon CSA (Figure 6A–c,f, B).

Depending on the repaired tissue type and quality, three distinct failure mechanisms were observed among the tested samples: midsection failure for scar-like repair tissue, and bony avulsion, or enthesis failure (specifically at the interface between the unmineralized and mineralized fibrocartilage, respectively) for tissues with a more regenerative healing response (Figure 7A,B). The native tissue failed via both catastrophic avulsion and enthesis failure modes (avulsion: enthesis failure, 50:50; Figure 7B). A similar combination of failure modes was seen in the PEG-IGF-1m treatment group (avulsion: enthesis failure; 25:75 at 4 weeks and 20:80 at 8 weeks, Figure 7B). The scar-like repair tissue in the rh-IGF-1 treatment group failed exclusively at the tendon mid-substance (100%, Figure 7B) along with a significant post-yield behavior (Figure 8A). In contrast, the repair control showed mixed modes of failure albeit with predominantly mid-substance failure at 8 weeks (avulsion:enthesis failure:midsubstance failure, 17:50:33 at 4 weeks, and 29:0:71 at 8 weeks, Figure 7B).

The regenerate tissue in the PEG-IGF-1m treatment group had sharper yield curves and their failure loads were approximately 69% and 90% of native rotator cuff tendon loads at 4 and 8 weeks, respectively (Figure 8B–a). This group also showed approximately 43% higher failure loads compared to the repair controls at 8 weeks ($p \leq .05$, Figure 8B–a). Likewise, the stiffness was approximately 55% higher ($p \leq .01$, Figure 8B–b) and work-to-failure was approximately 156% higher than the repair controls at 8 weeks ($p \leq .001$, Figure 8B–c), respectively. In line with these observations, there was significant improvement in tissues properties such as strength (approximately 44% and approximately 122% higher at 4 and 8 weeks) when compared to the repair control ($p \leq .05$ and .001 at 4 and 8 weeks, respectively) and reached approximately 60% of native tendon values by 8 weeks (Figure 8B–d). This was accompanied by an improvement in the Young's Modulus (approximately 20% and 63% at 4 and 8 weeks, respectively, ns, Figure 8B–e), and toughness, an indication of how much energy a material can absorb before rupturing. (approximately 10.5% and 60% at 4 and 8 weeks, $p \leq .001$ at 8 weeks, Figure 8B–f) compared to the repair controls rh-IGF-1 treatment group on the other hand showed detrimental healing outcomes with failure loads ~71% (at 4 weeks) and 61% (at 8 weeks) lower than the native tendon values ($p \leq .05$, Figure 8B–a). Likewise, there was also 85 and 89% reduction in stiffness at 4 and 8 weeks in the rh-IGF-1 treatment group when compared to native tendon ($p \leq .05$, Figure 8B–b). Similarly, there was significant reduction in tissues properties such as strength at both time points (approximately 80% reduction at 4 and 8 weeks, $p \leq .05$, respectively, Figure 8B–d), Young's Modulus (approximately 90% and 87% reduction at 4 and 8 weeks, $p \leq .05$, respectively, Figure 8B–e), and toughness (approximately 70 and 80% reduction at 4 and 8 weeks, $p \leq .05$, respectively, Figure 8B–f), when compared to the native tendon tissue.

4 | DISCUSSION

Our engineered PLA-CL matrices demonstrated controlled release of a structurally preserved model protein over the target period of 4 weeks, while simultaneously undergoing controlled degradation as reported in our earlier work.[25] The degradation byproducts or the

dispersion of lyophilized protein into the organic polymer-dissolved solvent phase did not result in significant polymer or solvent-induced structural perturbations of our model protein as noted by CD spectroscopic observation. This may be because of lesser conformational flexibility of a lyophilized protein when in an anhydrous organic solvent environment (compared to an aqueous/organic mixture), which preserves its secondary structure and prevents denaturation.[35] Hydrolytic breakdown of the polypeptide in the matrix interior may also be catalyzed by carboxylate or other acidic degradation products (low pH).[36] However, the lower LA content and the controlled degradation of the PLA:CL matrix enabled by slow degrading caprolactone may have resulted in less accumulation of acidic products and thereby helped maintain the protein conformation.[25] The tested matrices rapidly degraded by 4 weeks (~30%) due to preferential hydrolysis of the lactide-rich regions within the polymer, and subsequently maintained a stable molecular weight due to the emergence of highly crystalline caprolactone-rich regions.[25] The degradation over the 4-week period follows a near-linear trend. IGF-1 release was not assessed, however Model protein BSA release and water absorption showed a similar profile with respect to time indicating that diffusion may have primarily driven release.[25] For more information about water absorption, weight loss and model protein BSA release across a range of mol. Wt and casting concentrations, the reader is directed to our previous report.[25]

PEG-IGF-1m and IGF-1m and rh-IGF-1 were encapsulated independently within the optimized PLA-CL matrix for controlled delivery through the active tissue healing period of 4 weeks. Our work reports the first demonstration of the in vivo delivery and tissue repair response of pegylated-IGF-1 in the rotator cuff via a biodegradable polymeric matrix to achieve sustained and controlled delivery of these therapeutics. The PEG-IGF-1m treated groups demonstrated a distinct regenerative response in the rotator cuff, with improved tissue granulation and vascularity scores at both 4 and 8 weeks, an indication of reduced inflammation and improved wound healing in the repair tissue.[37] It also promoted the reestablishment of an organized fibrocartilaginous tissue along with the characteristic tidemark and interdigitating collagen fiber insertions, all hallmarks of the native tendon-to-bone insertion. Biomechanical assessment of the repaired rotator cuff tendon-to-bone interface showed that the mode of failure was strongly correlated to the tissue quality as previously reported.[38] The PEG-IGF-1m treatment group tissue failed at the enthesis (75% and higher) or by avulsion failure extending into the trabecular bone of the humeral head (20%–25%), like the native supraspinatus tendons that failed catastrophically by a 50:50 rate of avulsion versus enthesis failures. We also observed that the area of attachment avulsed was much smaller than the apparent attachment area in these groups tested, with denser fiber bundles found in the PEG-IGF-1m repair group tissue, as was also reported previously for healthy native tendon tissue.[38] On the other hand, the rh-IGF-1 treatment repair tissue was fibrotic and bulky with disorganized collagen that does not allow efficient load transfer and failed exclusively via mid-substance tears.

The two significant mechanical properties that are critical to prevent tears or retears of the rotator cuff tendon are strength and toughness (energy absorption capability of the tissue which protects against failure following onset of injury or retears post-repair).[38,39] The toughness of the PEG-IGF-1m treatment group tissue reached 80% native tendon toughness, whereas the repair controls tissue showed only 31% toughness values compared

to the native tendon. The toughness of the rh-IGF-1 treatment group tissue was even lower, reaching only 21% of native tendon values at 8 weeks. Although both repair controls and rh-IGF-1 treatment groups showed lower toughness compared to the native control and PEG-IGF-1m treatment groups, the rh-IGF-1 treatment group showed significantly more plastic deformation with very low Young's Modulus (approximately 13% of native tendon, $p \leq .05$, at 4 and 8 weeks, respectively) compared to repair control that exhibited a Young's Modulus of approximately 45% of native tendon, $p \leq .05$, at 4 and 8 weeks, respectively). Even with a higher displacement values the significantly low failure loads resulted in poor toughness in these groups. This and the significance post-yield behavior show that the deposited provisional tissue during repair did not get reinforced with strength as the tissue matured.

On the other hand, there was improvement in the toughness (78%, $p \leq .05$), strength (32%, ns), and Young's Modulus (33.83%, ns) in the PEG-IGF-1m treatment group as the tissue matured, although significant differences were only seen in the toughness values. The superior biomechanical properties of the PEG-IGF-1m treatment group agrees well with its structural regeneration seen histologically, in which an organized tendon and fibrocartilaginous enthesis with the tissue-typic columnar arrangement of fibrochondrocytes and interdigitating collagen fibers anchoring to cortical bone were observed at both 4 and 8 weeks. We also observed increasing collagen birefringence (a measure of tissue anisotropy) and distinct maturity pattern (increasing collagen fiber thickness) in the PEG-IGF-1 m-treatment group. Overall, the regeneration of this compliant zonal structure may have allowed efficient load transfer from the pliable tendon to the stiff bone. The organized collagen may absorb the load as energy and protect against retears.[38,40] The time point of healing is also critical as most retears occur within 3 months of repair.[3,41] Therefore, biological augmentation of rotator cuff repair using PEG-IGF-1m delivery may offer significant protection from retears during this critical time window.

This superior healing response in the pegylated growth factor mimic-treatment group than its bare IGF-1 analogue and the rh-IGF-1 may be due to a concentration-dependent immunomodulatory effect. IGF-1 has been shown to induce macrophage polarization to M2 macrophages which suppress inflammation by producing IL-10 and TGFβ.[18] However, at high concentrations, these factors maybe fibrotic in nature.[42] This is supported by previous studies in the literature, where equivalent dose of PEG-IGF-1 and rh-IGF-1 injection resulted in slow increase and sustained elevated serum concentration of PEG-IGF-1 compared to a transient increase and sharp drop in serum concentration of rh-IGF-1.[21] The large PEG residue slows association rates to IGF-1- and Insulin- receptor and IGF-I-binding proteins[21] to achieve this slow sustained activity. Therefore, the targeted IGF-1 release profile of slow controlled release without burst through the active tissue repair period of 4 weeks after injury may be achieved by the engineered matrix, with the pegylation furthering allowing slow activation of cells.[22] This controlled local delivery would further minimize any unnecessary systemic side effects. Another conducive factor maybe the improved bioactivity from increased stability of the insulin-like growth factor-1 provided by the pegylation[43] and encapsulation. Further studies are needed to gain insight into the potential released concentration-dependent tissue regenerative response.

This study is not without limitations. The first limitation is that the acute tear-repair model only represents a fraction of the rotator cuff injuries presented to the clinic and does not mimic chronic degenerative rotator cuff tendinopathy and injury.[14,44] However, there is increasing evidence of tears which are less degenerative and more trauma-based due to increase in activity levels in the older population.[45] Moreover, this rodent model is an established one for the pre-clinical testing of therapeutics.[12,46,47] The second is the exclusion of release study of IGF therapeutics. However, Since pegylation of IGF-1 has been shown to have therapeutic effect in muscle injury models, we designed the scope of the study to investigate any the potential regenerative effect of this factor delivery on repaired tendon-enthesis compared to its unpegylated controls. We observed improved remodeling of the collagen in PEG-IGF-1 versus other groups which is likely due to early inflammation-modulation on this tissue. Future studies evaluating the release of growth factor therapeutics during acute time points and its effect on modulating inflammation may provide us with key information needed to understand the pro-regenerative effect of pegylated IGF-1 delivery. Nevertheless, the objective of evaluating the tissue regenerative response of the released growth factor during critical stage of proliferation and early remodeling is sufficiently addressed in this study.[16,48]

5 | CONCLUSION

In summary, a surgically implantable biodegradable polymeric IGF-1 biotherapeutic delivery matrix showed controlled, localized, and conformationally stable delivery of model protein and promoted regenerative tissue healing of the complex enthesis within 8 weeks of repair. These results are significant as they provide impetus for translation of a single-growth factor delivery biomaterial device for the regenerative healing of the rotator cuff in patients with full-thickness tears. It also lays the ground-work for the repair of partial-thickness tears, which are two or three times more common than full-thickness rotator cuff tears[49] and have a 26% risk of tear progression within 2 years.[50] Our technology of using anabolic growth factors to promote neotendon and fibrocartilage formation may delay the progression of these tears to full-thickness and may provide an off-the-shelf surgically viable therapeutic option for the treatment of other fibrocartilaginous interfaces as well, such as in the temporomandibular joint.

Supplementary Material

Refer to Web version on PubMed Central for supplementary material.

ACKNOWLEDGMENTS

The authors acknowledge Novartis Grant G600795, University of Connecticut Office of the Vice President for Research Fund 401543, and the NIH Pioneer Grant 1DP1OD019349-01 for supporting this work. Anupama Prabhath acknowledges GE graduate fellowship grant for part-time research fellowship. The authors acknowledge Jean-Emmanuel Avochinou, Luis Loza Rojas, and Joanne Walker for helping assist in animal surgeries. The authors acknowledge Dr. Mark Maciejewski and Ms. Susan Staurovsky from the University of Connecticut, CT, USA for their technical support with circular dichroism spectroscopy and confocal microscopy, respectively. The authors acknowledge Dr. Louis Soslowsky, McKay Orthopedic Research Laboratory at The University Of Pennsylvania, PA, USA for training Varadraj N. Vernekar on the rat rotator cuff surgery. Furthermore, the authors acknowledge Ms. Jennica Tucker and Ms. Courtney Nuss (from Dr. Louis Soslowsky's laboratory), Dr. Mikhail Golman (from Dr. Stavros Thomopoulos's laboratory at Columbia University, NY, USA), Ms. Paige Woods (from Dr. Tannin Schmidt's laboratory at UConn Health, CT, USA), and Drs. Scott Rodeo and Xiang-Hua Deng from the Hospital

for Special Surgery, NY, USA for guidance on the rat rotator cuff surgery. The authors acknowledge Dr. Chang Hun Lee and Dr. Solaiman Tarafder at College of Dental Medicine, Columbia University, NY, USA for help with circularly polarized microscopy. The authors also acknowledge the Center for Comparative Medicine at UConn Health, CT, USA for assistance with the in vivo study, Renata Rydzik for assistance in microCT analyses, and Nancy Troiano from the Yale Orthopedic Histology and Histomorphometry Laboratory, Yale University, CT, USA for assistance with histology.

Funding information

NIH Pioneer, Grant/Award Number: 1DP1OD019349-01; Novartis, Grant/Award Number: G600795; National Institute of Arthritis and Musculoskeletal and Skin Diseases Ruth L. Kirschstein National Research Service Award (NRSA) Institutional Research Training Grant, Grant/Award Number: 1T32AR079114-01

DATA AVAILABILITY STATEMENT

The data that support the findings of this study are available from the corresponding author upon reasonable request.

REFERENCES

1. Novakova SS, Mahalingam VD, Florida SE, et al. Tissue-engineered tendon constructs for rotator cuff repair in sheep. J Orthop Res 2018; 36:289–299. [PubMed: 28657154]
2. Pedowitz RA, Yamaguchi K, Ahmad CS, Burks RT, et al. Optimizing the management of rotator cuff problems. JAAOS 2011;19: 368–379. [PubMed: 21628648]
3. Galatz LM, Ball CM, Teefey SA, Middleton WD, Yamaguchi K. The outcome and repair integrity of completely arthroscopically repaired large and massive rotator cuff tears. JBJS 2004;86:219–224.
4. Derwin KA, Baker AR, Iannotti JP, McCarron JA. Preclinical models for translating regenerative medicine therapies for rotator cuff repair. Tissue Eng Part B Rev 2010;16:21–30. [PubMed: 19663651]
5. Apostolakos J, Durant TJ, Dwyer CR, et al. The enthesis: a review of the tendon-to-bone insertion. Muscles Ligam Tendons J 2014;4: 333–342.
6. Cummins CA, Murrell GAC. Mode of failure for rotator cuff repair with suture anchors identified at revision surgery. J Shoulder Elbow Surg 2003;12:128–133. [PubMed: 12700563]
7. Prabhath A, Vernekar VN, Sanchez E, Laurencin CT. Growth factor delivery strategies for rotator cuff repair and regeneration. Int J Pharm 2018;544:358–371. [PubMed: 29317260]
8. Kovacevic D, Fox AJ, Bedi A, et al. Calcium-phosphate matrix with or without tgf-β3 improves tendon-bone healing after rotator cuff repair. Am J Sports Med 2011;39(4):811–819. [PubMed: 21406666]
9. Manning CN, Kim HM, Sakiyama-Elbert S, Galatz LM, Havlioglu N, Thomopoulos S. Sustained delivery of transforming growth factor beta three enhances tendon-to-bone healing in a rat model. J Orthop Res 2011;29:1099–1105. [PubMed: 21246611]
10. Zhao S, Zhao J, Dong S, et al. Biological augmentation of rotator cuff repair using bFGF-loaded electrospun poly (lactide-co-glycolide) fibrous membranes. Int J Nanomed 2014;9:2373.
11. Liu W, Lipner J, Xie J, Manning CN, Thomopoulos S, Xia Y. Nanofiber scaffolds with gradients in mineral content for spatial control of osteogenesis. ACS Appl Mater Interfaces 2014;6:2842–2849. [PubMed: 24433042]
12. Lipner J, Shen H, Cavinatto L, et al. In vivo evaluation of adipose-derived stromal cells delivered with a nanofiber scaffold for tendon-to-bone repair. Tissue Eng Part A 2015;21:2766–2774. [PubMed: 26414599]
13. Peach MS, Ramos DM, James R, et al. Engineered stem cell niche matrices for rotator cuff tendon regenerative engineering. PLoS One 2017;12:e0174789. [PubMed: 28369135]
14. Tang X, Saveh Shemshaki N, Vernekar VN, et al. The Treatment of Muscle Atrophy After Rotator Cuff Tears Using Electroconductive Nanofibrous Matrices. Regen Eng Transl Med 2021;7(1):1–9. [PubMed: 33816776]

15. Wurgler-Hauri CC, Dourte LM, Baradet TC, Williams GR, Soslowsky LJ. Temporal expression of 8 growth factors in tendon-to-bone healing in a rat supraspinatus model. J Shoulder Elbow Surg 2007;16:S198–S203. [PubMed: 17903711]
16. Kobayashi M, Itoi E, Minagawa H, et al. Expression of growth factors in the early phase of supraspinatus tendon healing in rabbits. J Shoulder Elbow Surg 2006;15:371–377. [PubMed: 16679241]
17. Ichinose T, Lesmana R, Yamamoto A, et al. Possible involvement of IGF-1 signaling on compensatory growth of the infraspinatus muscle induced by the supraspinatus tendon detachment of rat shoulder. Physiol Rep 2014;2:e00197. [PubMed: 24744876]
18. Tonkin J, Temmerman L, Sampson RD, et al. Monocyte/macrophage-derived IGF-1 orchestrates murine skeletal muscle regeneration and modulates autocrine polarization. Mol Ther 2015;23:1189–1200. [PubMed: 25896247]
19. Kurtz CA, Loebig TG, Anderson DD, DeMeo PJ, Campbell PG. Insulin-like growth factor I accelerates functional recovery from Achilles tendon injury in a rat model. Am J Sports Med 1999;27:363–369. [PubMed: 10352775]
20. Morimoto LM, Newcomb PA, White E, Bigler J, Potter JD. Variation in plasma insulin-like growth factor-1 and insulin-like growth factor binding Protein-3: genetic factors. Cancer Epidemiol Biomark Prev 2005;14:1394–1401.
21. Metzger F, Sajid W, Saenger S, et al. Separation of fast from slow anabolism by site-specific PEGylation of insulin-like growth factor I (IGF-I). J Biol Chem 2011;286:19501–19510. [PubMed: 21460230]
22. Parker K, Berretta A, Saenger S, et al. PEGylated insulin-like growth factor-I affords protection and facilitates recovery of lost functions post-focal ischemia. Sci Rep 2017;7:241. [PubMed: 28325900]
23. Saenger S, Goeldner C, Frey JR, et al. PEGylation enhances the therapeutic potential for insulin-like growth factor I in central nervous system disorders. Growth Horm IGF Res 2011;21:292–303. [PubMed: 21865068]
24. Estey T, Kang J, Schwendeman SP, Carpenter JF. BSA degradation under acidic conditions: a model for protein instability during release from PLGA delivery systems. J Pharm Sci 2006;95:1626–1639. [PubMed: 16729268]
25. Prabhath A, Vernekar VN, Vasu V, et al. Kinetic degradation and biocompatibility evaluation of polycaprolactone-based biologics delivery matrices for regenerative engineering of the rotator cuff. J Biomed Mater Res A 2021;109:2137–2153. [PubMed: 33974735]
26. Fu K, Pack DW, Klibanov AM, Langer R. Visual evidence of acidic environment within degrading poly (lactic-co-glycolic acid) (PLGA) microspheres. Pharm Res 2000;17:100–106. [PubMed: 10714616]
27. Park MC, Cadet ER, Levine WN, Bigliani LU, Ahmad CS. Tendon-to-bone pressure distributions at a repaired rotator cuff footprint using transosseous suture and suture anchor fixation techniques. Am J Sports Med 2005;33:1154–1159. [PubMed: 16000662]
28. Ide J, Kikukawa K, Hirose J, Iyama K-i, Sakamoto H, Mizuta H. The effects of fibroblast growth factor-2 on rotator cuff reconstruction with acellular dermal matrix grafts. Arthrosc: J Arthrosc Relat Surg 2009;25:608–616.
29. Jensen EC. Quantitative analysis of histological staining and fluorescence using ImageJ. Anat Rec 2013;296:378–381.
30. Greiner C, Grainger S, Farrow S, et al. Robust quantitative assessment of collagen fibers with picrosirius red stain and linearly polarized light as demonstrated on atherosclerotic plaque samples. PLoS One 2021; 16:e0248068. [PubMed: 33735190]
31. Saitta Rezakhaniha R, Agianniotis A, Schrauwen J, et al. Experimental investigation of collagen waviness and orientation in the arterial adventitia using confocal laser scanning microscopy. Biomech Model Mechanobiol 2011;11:461–473. [PubMed: 21744269]
32. Golman M, Li X, Skouteris D, et al. Enhanced tendon-to-bone healing via IKKβ inhibition in a rat rotator cuff model. Am J Sports Med 2021; 49(3):780–789. [PubMed: 33507808]
33. Norton DR, Keller A. The spherulitic and lamellar morphology of melt-crystallized isotactic polypropylene. Polymer 1985;26(5):704–716.

34. Ozkan S, Kalyon DM, Yu X, McKelvey CA, Lowinger M. Multifunctional protein-encapsulated polycaprolactone scaffolds: fabrication and in vitro assessment for tissue engineering. Biomaterials 2009;30:4336–4347. [PubMed: 19481253]
35. Acharya AS, Iyer KS, Sahni G, Khandke KM, Manjula BN. Restriction in the conformational flexibility of apoproteins in the presence of organic cosolvents: a consequence of the formation of “native-like conformation”. J Protein Chem 1992;11:527–538. [PubMed: 1333215]
36. Lu W, Park TG. Protein release from poly(lactic-co-glycolic acid) microspheres: protein stability problems. PDA J Pharm Sci Technol 1995;49:13–19. [PubMed: 7757453]
37. Howell K, Chien C, Bell R, et al. Novel model of tendon regeneration reveals distinct cell mechanisms underlying regenerative and fibrotic tendon healing. Sci Rep 2017;7:45238. [PubMed: 28332620]
38. Mikhail Golman AA, Kurtaliaj I, Marshall B, et al. Toughening mechanisms for the attachment of architectured materials: The mechanics of the tendon enthesis. Sci Adv 2021;7:48.
39. Newton JB, Fryhofer GW, Rodriguez AB, Kuntz AF, Soslowsky LJ. Mechanical properties of the different rotator cuff tendons in the rat are similarly and adversely affected by age. J Biomech 2021;117: 110249. [PubMed: 33486263]
40. Linderman SW, Golman M, Gardner TR, et al. Enhanced tendon-to-bone repair through adhesive films. Acta Biomater 2018;70:165–176. [PubMed: 29427745]
41. Harryman DT 2nd, Mack LA, Wang KY, Jackins SE, Richardson ML, Matsen FA 3rd. Repairs of the rotator cuff. Correlation of functional results with integrity of the cuff. J Bone Joint Surg Am 1991;73: 982–989. [PubMed: 1874784]
42. Morita W, Snelling SJB, Wheway K, et al. ERK1/2 drives IL-1β-induced expression of TGF-β1 and BMP-2 in torn tendons. Sci Rep 2019;9:19005. [PubMed: 31831776]
43. Lawrence PB, Price JL. How PEGylation influences protein conformational stability. Curr Opin Chem Biol 2016;34:88–94. [PubMed: 27580482]
44. Killian ML, Cavinatto LM, Ward SR, Havlioglu N, Thomopoulos S, Galatz LM. Chronic degeneration leads to poor healing of repaired massive rotator cuff tears in rats. Am J Sports Med 2015;43:2401–2410. [PubMed: 26297522]
45. Paloneva J, Lepola V, Äärimaa V, Joukainen A, Ylinen J, Mattila VM. Increasing incidence of rotator cuff repairs–a nationwide registry study in Finland. BMC Musculoskelet Disord 2015;16:189. [PubMed: 26265152]
46. Derwin KA, Galatz LM, Ratcliffe A, Thomopoulos S. Enthesis repair: challenges and opportunities for effective tendon-to-bone healing. J Bone Jt Surg 2018;100:e109.
47. Galatz L, Rothermich S, VanderPloeg K, Petersen B, Sandell L, Thomopoulos S. Development of the supraspinatus tendon-to-bone insertion: localized expression of extracellular matrix and growth factor genes. J Orthop Res 2007;25:1621–1628. [PubMed: 17600822]
48. Thomopoulos S, Parks WC, Rifkin DB, Derwin KA. Mechanisms of tendon injury and repair. J Orthop Res 2015;33:832–839. [PubMed: 25641114]
49. Sher JS, Uribe JW, Posada A, Murphy BJ, Zlatkin MB. Abnormal findings on magnetic resonance images of asymptomatic shoulders. J Bone Joint Surg Am 1995;77:10–15. [PubMed: 7822341]
50. Kim D, Kim Y-S, Lee H-J, et al. Tear progression of symptomatic full-thickness and partial-thickness rotator cuff tears as measured by repeated MRI. Art Ther 2017;33:e52–e53.

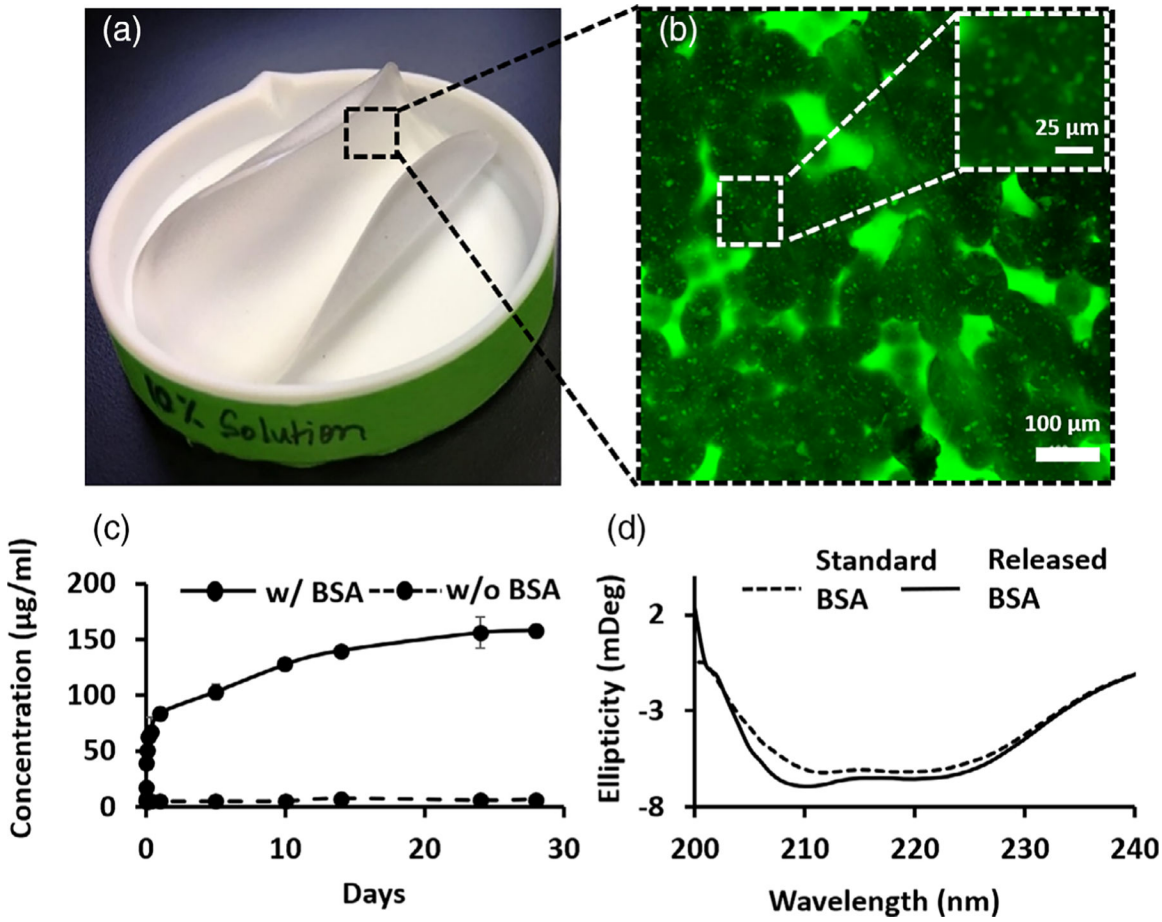

FIGURE 1.

Engineered polymeric matrices are highly flexible and porous and offer controlled release of the protein payload while helping maintain native protein conformation. (A) Flexible thin-film-based matrices were fabricated via a solvent evaporation process in Teflon evaporation dishes. (B) Interconnected porous microstructure of the fabricated matrix with encapsulated protein particles present within the fused copolymeric microspherules (porosity is indicated by the surrounding green regions that are accessible to fluorescein solution); inset shows magnified image of microspherules with dispersed protein particles stained punctate green therein via infiltration of fluorescein solution (which was not observed in controls without encapsulated protein). (C) Model protein Bovine Serum Albumin (BSA) was released from the engineered matrices in a controlled manner over 4 weeks. $n = 3$ samples/timepoint. (D) Released protein conformation was close to model protein even as late as 8 weeks as measured via circular dichroism spectroscopy, $n = 3$ samples

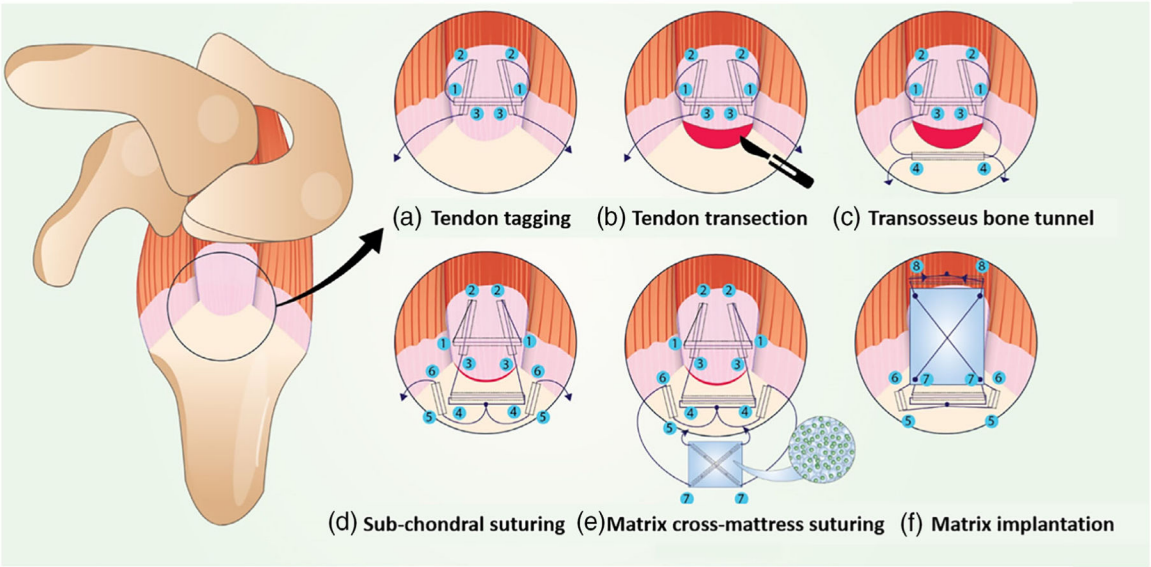

FIGURE 2.

Modified Mason Allen suturing technique to implant the growth factor delivery polymeric matrix for rotator cuff repair and the gross morphological observation of the implanted and the remodeled matrix. The rotator cuff supraspinatus tendon was exposed by retracting the overlying deltoid muscle. (A) The supraspinatus (SS) tendon was tagged using a transverse suture which was introduced posterior to anterior, approximately 3 mm from the insertion. A second loop was passed with the anterior limb of the suture from medial to lateral, extra- (top) to intra- (bottom) articular through the anterior portion of the supraspinatus tendon, taking care to catch the transverse limb. This pass was replicated with the posterior limb of the suture. (B) The supraspinatus tendon from the humeral head was released by a sharp transection using a #11 blade and was separated from the neighboring infraspinatus and subscapularis tendons to expose the articular surface of the humeral head. (C) The humeral head was debrided with a surgical bur to remove any residual tendon left behind at the insertion footprint after transection. A bone tunnel was drilled through the greater tuberosity beginning at a site approximately 2 mm lateral to the articular surface and 2 mm distal to the supraspinatus tendon footprint. This tunnel was transverse from the posterior to the anterior along the superior border of the greater tuberosity and opened at a distal site above the subscapularis taking care not to damage other tendons during the process. The sutures were passed antero-posteriorly and vice versa through the bone tunnel. (D) The emerging suture limbs were tied down via five knots–first surgeon's knot (two loops) + four regular knots. The emerging anterior suture limb from the knot was passed sub-chondrally from the proximal to the distal aspect of the greater tuberosity. This pass was replicated with the posterior limb of the suture. (E) The sub-chondrally emerging limbs were passed inferio-distally to emerge proximally in the opposite direction to create a cross-mattress stitch on the polymeric matrix. This flips the matrix during localization and ensures that the plain side of the matrix (without the cross-mattress suture) opposes the tendon surface. (F) The emerging suture ends from the matrix were used to create a transverse pass through the tendon mid-section and tied. Thus, the matrix was implanted as a non-load bearing

“piggy-back” patch on the bursal side of the supraspinatus tendon-to-bone insertion site. AC, acromion; SS, supraspinatus; IS, infraspinatus; SC, subscapularis; H, humerus

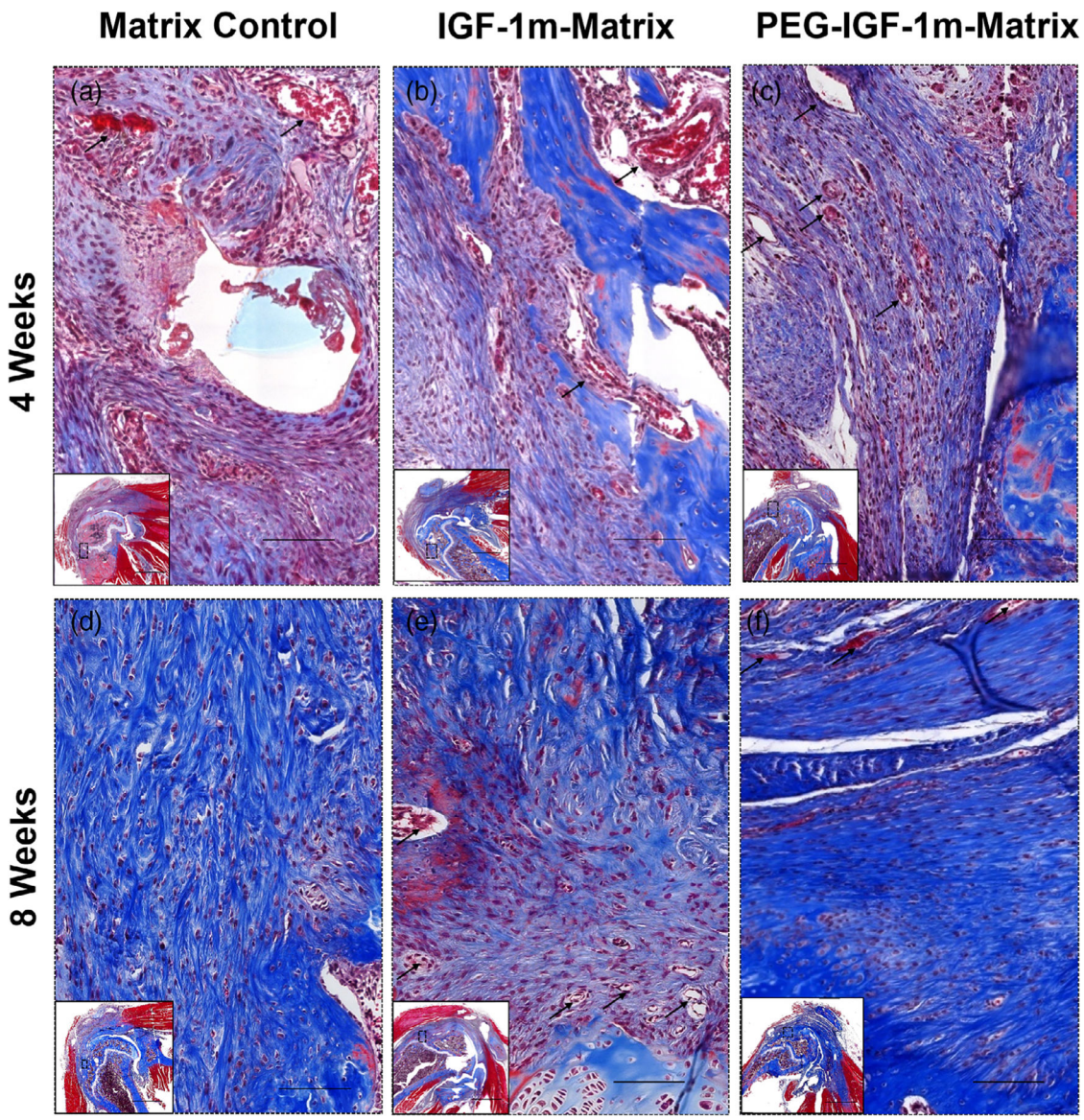

FIGURE 3.

Rotator cuff tendon-to-bone interface tissue repair response. Representative Masson's trichrome-stained sections of Matrix Control (A and D), IGF-1m Matrix (B and E), and PEG-IGF-1m Matrix (C and F) treatment groups at 4 and 8 weeks, respectively. At 4 weeks the tendon-to-bone interface in all the repair groups was populated with higher number of cells and blood vessels indicative of the normal wound healing response (black arrows indicate blood vessels); (A–C) At 8 weeks, the tendon-to-bone interface remodeled to more organized tissue (D–F); however, the PEG-IGF-1m treatment group (f) showed formation of highly dense, well-oriented collagen, and organized fibrocartilaginous tissue. $n = 3$ tissue samples/group at 4 weeks and $n = 4$ tissue samples/group at 8 weeks; 3–4 consecutive sections at similar sample depths were tissue landmarks namely growth plate pattern, shape of humerus, and supraspinatus tendon footprint was nearly identical was chosen for evaluations. Scale bar 100 μm

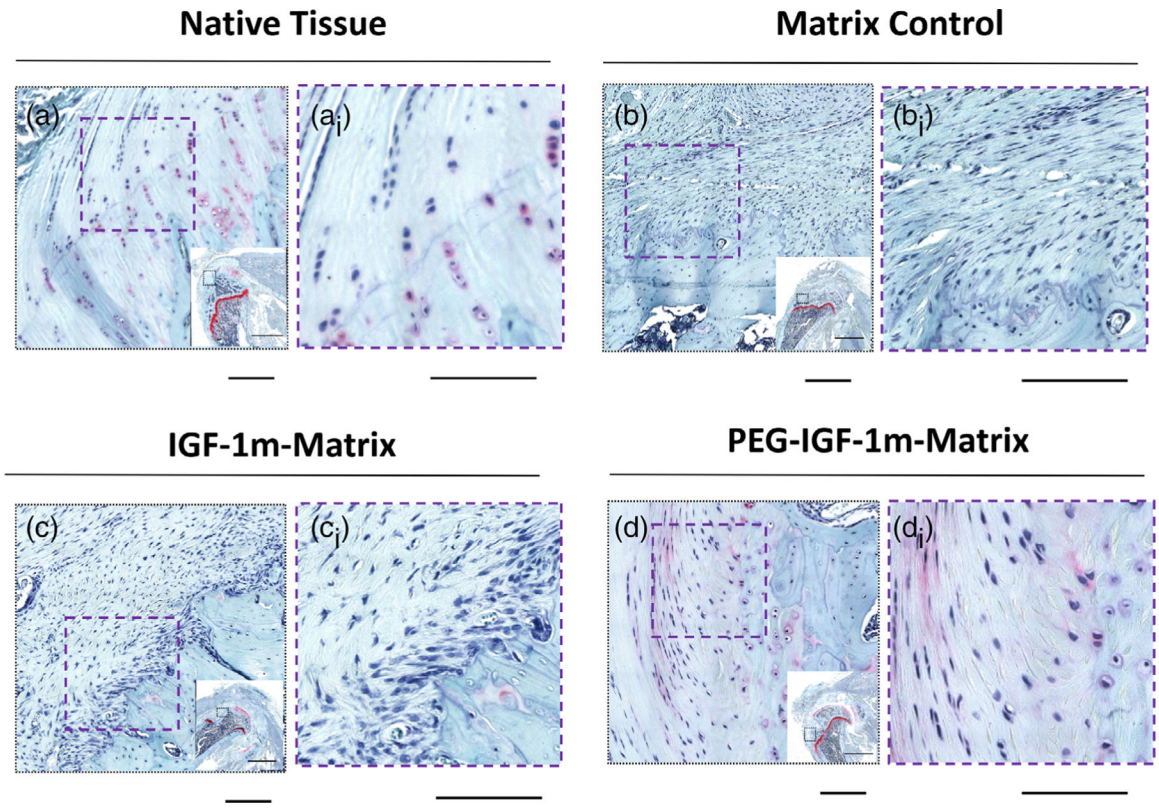

FIGURE 4.

Formation of fibrocartilaginous tissue at the repair interface. Representative Safranin O-stained sections showing the region of interest in (A, A_i) Native Tissue, (B, B_i) Matrix Control, (C, C_i) IGF-1m Matrix, and (D, D_i) PEG-IGF-1m Matrix treatment groups at 8 weeks. As can be seen, highly organized fibrocartilaginous tissue was observed along with its characteristic columnar arrangement of fibrochondrocytes, minimal metachromasia, and tidemark only in the PEG-IGF-1m treatment group (D, D_i) closely resembling native tissue (A, A_i). n = 4 tissue samples/group. Scale bar 100 μm

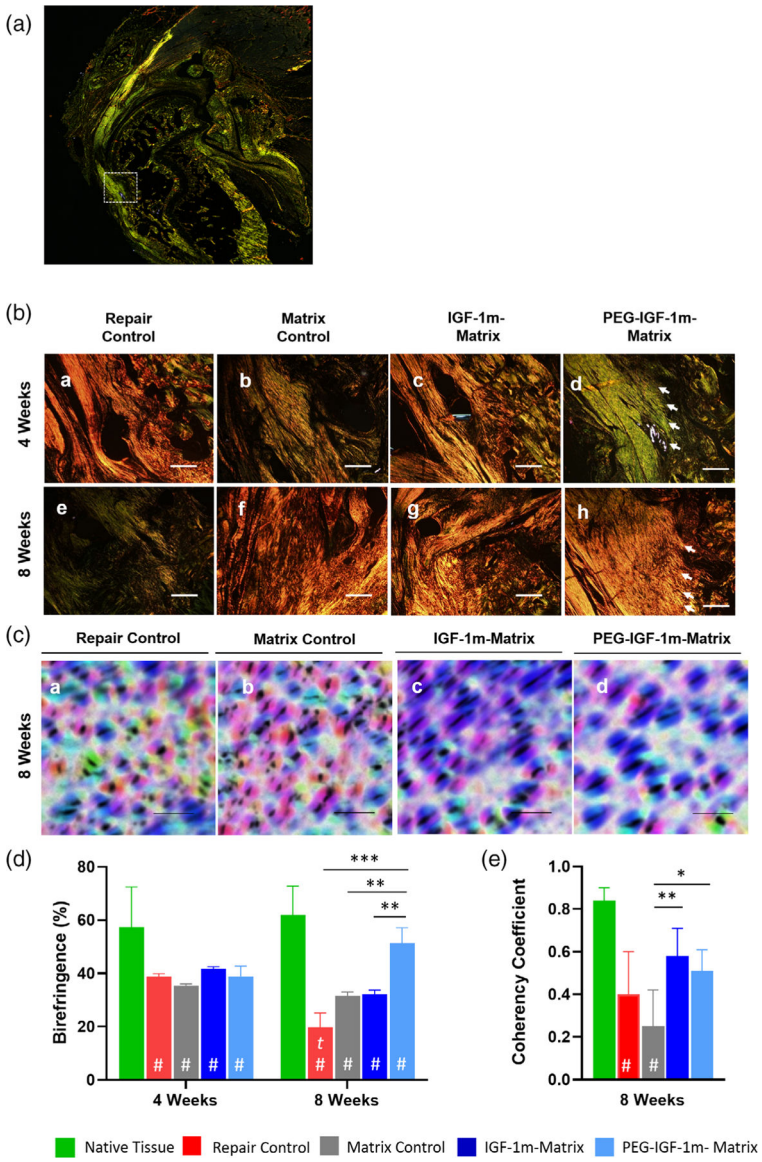

FIGURE 5.

Polarized light imaging of Picrosirius Red stained sections at the enthesis showed robust collagen organization in IGF-1 mimics treated groups compared to the repair and matrix controls at 4 and 8 weeks. (A) Representative low-magnification figure shows selection of the enthesis region of interest. (B) Representative images showing collagen organization in Picrosirius Red-stained cross sections of the repair groups at 4 (A–D) and 8 (E–H) weeks at 40× objective; scale bar–500 μm), respectively. The organized collagen appears brighter than the disorganized collagen because of higher polarization and diffraction of light. White arrows indicate collagen fibers inserting into bone in the PEG-IGF-1m treatment group. (C) Representative Safranin O-stained images showing cell orientation (color-coded by direction) of the repaired groups at 8 weeks as illustrated using orientationJ, an imageJ plug-in. Higher directionality (the majority of cells with the same color code) was seen in the IGF-1 mimics treated groups (C, D) compared to controls (A, B), scale bar 100 μm.

(D) Semi-quantitative evaluation of collagen birefringence using two representative regions of interest (ROIs) of 250 μm^2 for each replicate of Picrosirius Red-stained images was performed via ImageJ. (E) Quantification of coherency coefficient values reflecting cell orientation as illustrated in the images in (C) showed significant dominant directionality for the cells in the IGF-1 mimics treated groups compared to the matrix control (*$p \leq .05$, 2-way ANOVA with Tukey's multiple comparisons post-hoc test). Error bars represent standard deviation. $n = 3$ tissue samples/group at 4 weeks and four tissue samples/group at 8 weeks; 3–4 consecutive sections at similar sample depths were chosen for evaluations

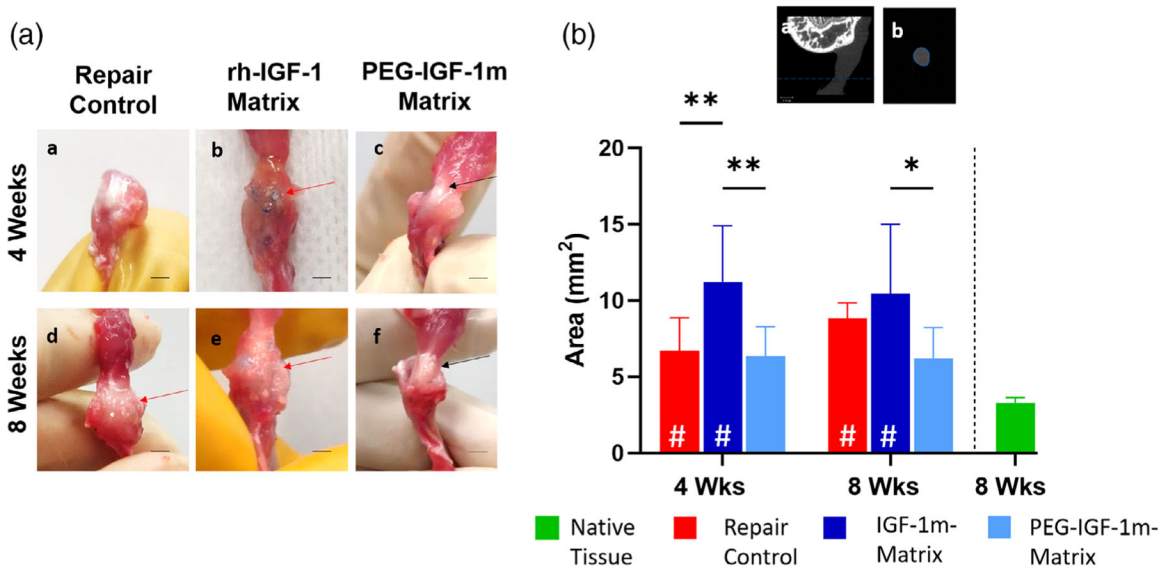

FIGURE 6.

Scar versus regenerative tissue healing in rh-IGF-1 versus PEG-IGF-1m Treatment Groups. (A) Diagnostic necropsy of representative repaired rotator cuff samples showing gross morphology of the repaired interface. rh-IGF-1 and PEG-IGF-1m treatment groups demonstrated distinctly different repair responses with the former healing with a larger cross-sectional area (CSA) scar tissue (red arrows in A-b, e) compared to the smaller CSA regenerate "tendon-like" whitish tissue seen in the latter (black arrows in A-c, f). Repair control also exhibited higher CSA scar tissue at 8 weeks (red arrow in A-d). (B) Minimum CSA quantified from microCT images. Representative coronal- (a) and transverse- (b) section images of a rotator cuff tendon from microCT (tendon is seen as the uniformly dimly lit gray region). The smallest transverse section area is used to quantify the minimum CSA shown in the graph. Two-way ANOVA followed by the Tukey's post hoc test was used to compare the treatment groups and controls for significant differences. Significant differences compared to native rat rotator cuff tissue are indicated by "#" within the bar; (*$p \leq .05$, **$p \leq .01$). $n = 6–8$ tissue samples/group/timepoint were used for analysis in B

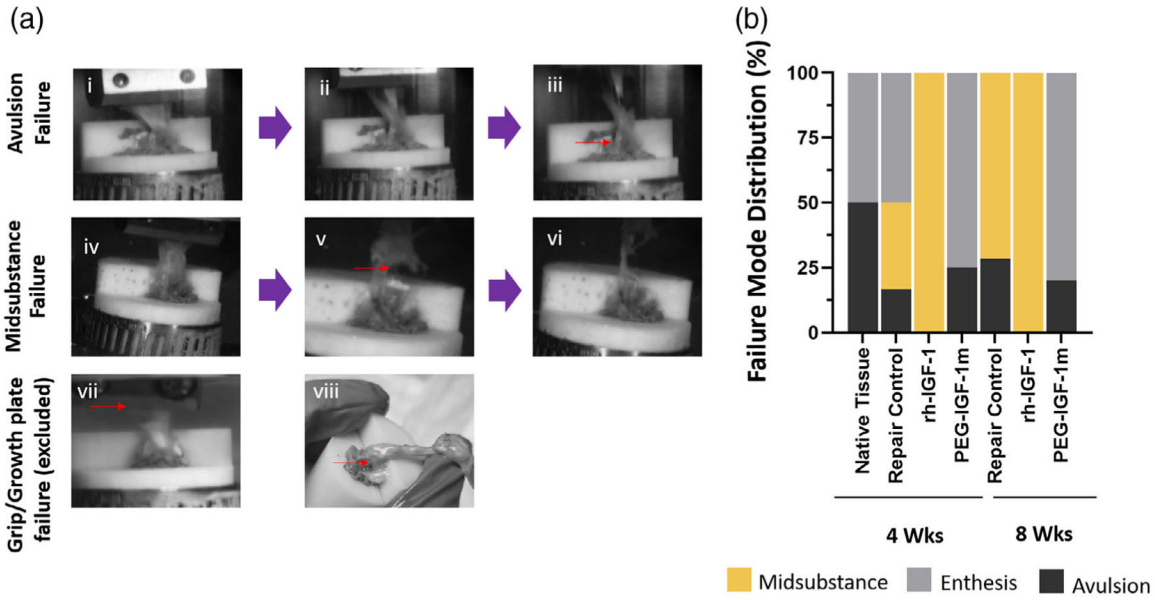

FIGURE 7.

Distinct Failure Modes and Distribution in the Repaired Rotator Cuff Insertions. (A) The repaired rat supraspinatus enthesis exhibited two distinct failure modes: bony avulsion/enthesis failures (A_i–A_{iii}) and tendon midsubstance failure (A_{iv}–A_{vi}) depending on repaired tissue characteristics. The tissues that failed with either grip failure or growth plate fracture was excluded from the study (A_{vii}, A_{viii}). (B) Failure mode distributions showed exclusive midsubstance failure in the rh-IGF-1 treatment group (100% at 4 and 8 weeks, respectively) that had fibrotic repaired tissue, a mixture of midsubstance and avulsion/enthesis failure in repair controls (Midsubstance: Enthesis: Avulsion = 33:50:17 at 4 weeks and 29:0:71 at 8 weeks, respectively), and predominant avulsion/enthesis failure in the PEG-IGF-1m treatment group (Enthesis: Avulsion = 25:75 at 4 weeks and 20:80 at 8 weeks, respectively) similar to the native rat rotator cuff tissue (Enthesis: Avulsion = 50:50). n = 6–8 tissue samples/group/timepoint were used for analysis in B

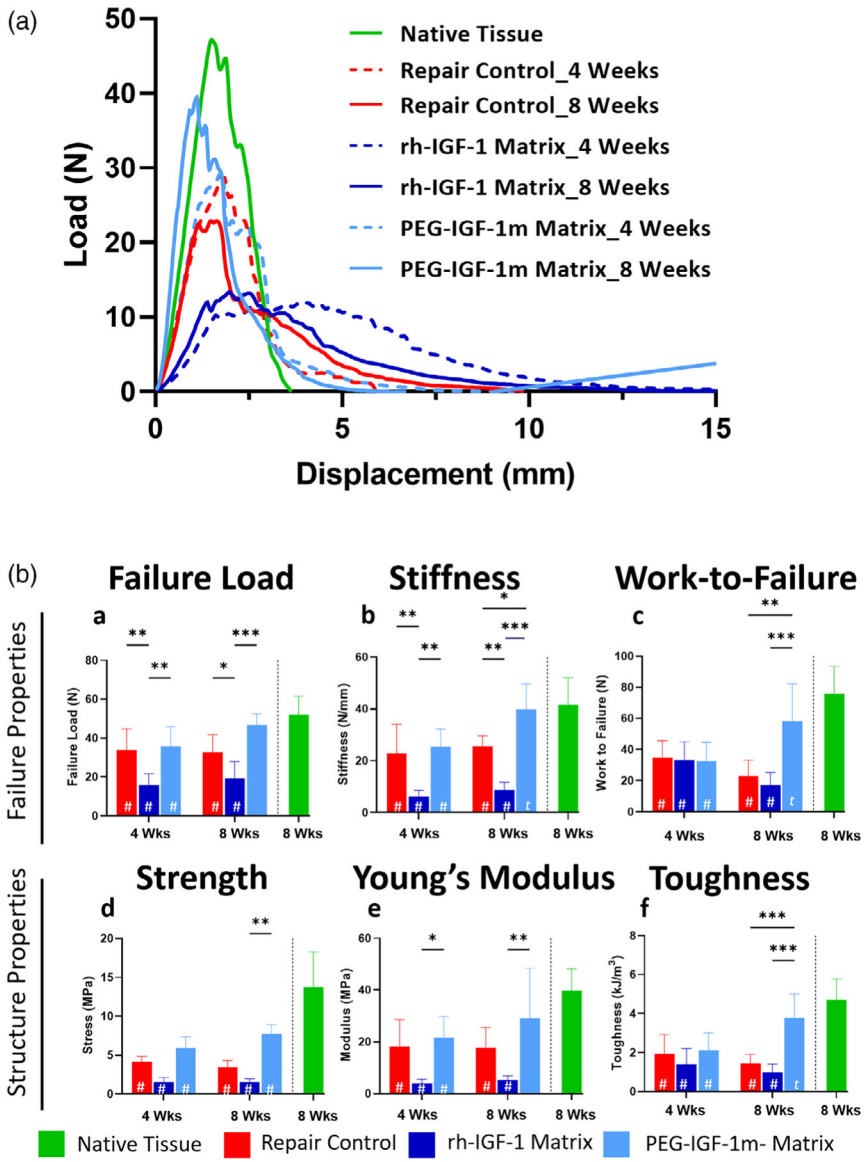

FIGURE 8.

Treatment with the PEG-IGF-1m matrix significantly improved failure and material properties of the tendon at 4 weeks and 8 weeks of healing compared to the repair controls and rh-IGF-1 matrix repair groups. (A) Load versus displacement curves of repair control and treatment groups at 4 (dotted lines) and 8 (solid lines) weeks using mean ordinance method on OriginPro 9. The rh-IGF-1 matrix group (dark blue) showed broader load versus displacement curves, extensive post-yield behavior, and failure at lower loads at both 4 and 8 weeks when compared to repair control (red) and PEG-IGF-1m (light blue). The latter showed significantly improved failure loads reaching approximately 80% of the native rotator cuff control failure loads by 8 weeks. B (a–c) Failure properties of the different treatment and control groups calculated from the load versus displacement curves. B (d–f) Structural properties of the different treatment and control groups calculated from the stress–strain curves. Two-way ANOVA followed by the Tukey's post hoc test was used to

compare for significant differences between the treatment groups and controls. Significance differences compared to native rat rotator cuff tissue are indicated by "#" within the bar; (*$p \leq .05$, **$p \leq .01$; ***$p \leq .001$. A significant difference ($p \leq .05$) between timepoints is indicated by "t" within the bar. $n = 6–8$ tissue samples/group/timepoint were used for analysis in B

TABLE 1

Modified tendon-to-bone insertion maturity scoring key and scores at 4 and 8 weeks

	1	2	3	4
Granulation tissue	<25%	26%–50%	51%–75%	>75%
Vascularity	<6 BV/low PF	6–10 BV/low PF	11–15 BV/low PF	15 BV/low PF
Cellularity	Minimal	Mild	Moderate	Marked
Insertion integrity	C(+) R(+) F(+)	C(+) R(+) F(−)	C(+) R(−) F(−)	C(−) R(−) F(−)
Maturity	Sum of scores indication of insertion maturity (4–normal; 16–farthest from normal)			

Note: (A) The histological scoring for rotator cuff tendon-to-bone insertion maturity was adapted from Lipner et al.[12] Each outcome was scored from 1 (closest to normal) to 4 (abnormal). Sum of the scores gives an indication of enthesis maturity (4–normal; 16–farthest from normal). (B) Histomorphometry at the tendon-to-bone insertion showed an improved score closest to the native tissue only in the PEG-IGF-1m treatment group reflecting the qualitative observations. Data are presented as median (range). $n = 3$ tissue samples/group at 4 weeks and 4 tissue samples/group at 8 weeks; 3–4 consecutive sections was chosen for evaluations.

J Biomed Mater Res A. Author manuscript; available in PMC 2023 July 06.

TABLE 2

Histological scores of tendon-to-bone insertions using modified scoring key in Table 1

	4 Weeks					8 Weeks				
	Sham	**Repair control**	**Matrix control**	**IGF-1m matrix**	**PEG-IGF-1m matrix**	**Sham**	**Repair control**	**Matrix control**	**IGF-1m matrix**	**PEG-IGF-1m matrix**
Granulation tissue	1 (1, 1)	1 (1, 1)	2 (2, 2)	1 (1, 1)	1 (1, 1)	1 (1, 1)	1 (1, 2)	1 (1, 1)	1 (1, 1)	1 (1, 2)
Vascularity	1 (1, 1)	1 (1, 1)	3 (2, 4)	2 (1, 3)	1 (1, 1)	1 (1, 1)	3 (1, 4)	2 (1, 4)	3 (2, 3)	1 (1, 4)
Cellularity	1 (1, 1)	4 (4, 4)	4 (4, 4)	4 (4, 4)	4 (4, 4)	1 (1, 2)	3 (3, 4)	3 (3, 4)	3 (3, 4)	3 (2, 3)
Insertion integrity	1 (1, 1)	3 (2, 4)	3 (2, 3)	3 (2, 3)	3 (3, 3)	1 (1, 1)	1 (1, 2)	3 (1, 4)	3 (1, 4)	1 (1, 2)
Maturity	4 (4, 4)	9 (8, 10)	12 (10, 13)	10 (8, 11)	9 (9, 9)	4 (4, 5)	8 (6, 12)	9 (6, 13)	10 (7, 12)	6 (5, 11)

Note: Histomorphometry at the tendon-to-bone insertion showed an improved score closest to the native tissue only in the PEG-IGF-1m treatment group reflecting the qualitative observations. Data are presented as median (range). $n = 3$ tissue samples/group at 4 weeks and four tissue samples/group at 8 weeks; 3–4 consecutive sections was chosen for evaluations. BV, blood vessels; PF, power field; C, continuity; R, regularity; F, fibrocartilage.